

Reinforced Hydroxylated Boron Nitride on Porous Sulfonated Poly(ether sulfone) with Excellent Electrolyte Properties for H₂/O₂ Fuel Cells

Gayathri Ravi Kumar, Raja Pugalenti M, Guozhong Cao, and Ramesh Prabhu Manimuthu*



Cite This: *Energy Fuels* 2022, 36, 6445–6458



Read Online

ACCESS |



Metrics & More

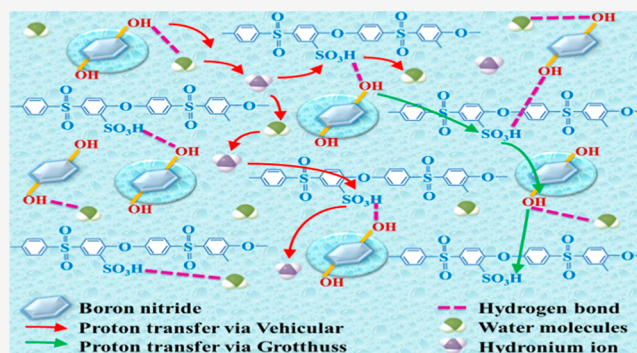


Article Recommendations



Supporting Information

ABSTRACT: Designing a high-performing amorphous porous framework of the proton-conducting membrane with inherent SO₃H moieties in the aromatic chain and impregnating the proton source is beneficial for developing an excellent electrolyte for the proton exchange membrane fuel cell. In this work, we synthesize the porous sulfonated poly(ether sulfone) (PSPES) nanocomposite membranes with excellent proton conductivity and stability via modified non-solvent-induced phase inversion. The hydroxylated boron nitride (HBN) was prepared from the bulk BN through simple liquid exfoliation and hydroxylation, which yielded the few-layered sheets. The direct inclusion of HBN into the PSPES will be anchoring or filling on the microporous channels of the membrane, yielding outstanding stability with HBN retention ability and high conductivity. Thereby, an excellent synergistic effect between the PSPES and HBN through the functional groups (SO₃H–OH) is shown, producing the proton transport bridge and continuous proton transfer channels within the porous structure. Besides, the current and power density of the 3.5 wt % HBN reinforced PSPES (PSPES-HBN2) membranes were improved to 795 mA cm⁻² and 220 mW cm⁻². The interconnected microporous PSPES-HBN2 membrane shows an excellent proton conductivity of 77.4 ± 3.87 mS cm⁻¹ at 80 °C with 100% humidity and notably reduced membrane degradation after a 120 h durability test.



1. INTRODUCTION

Global energy demand for the continuing population growth and industrial development will increase further in the upcoming decades. Alternative clean, renewable energy sources such as fuel cells are the best choice for tackling the issues of fossil fuels. The next generation of energy-saving is the hydrogen fuel cell that converts the chemical energy stored in fuel into instant electrical energy rather than a combustion reaction. It is chosen as the next power source in contrast to other energy storages due to its rapid start-up, higher reaction kinetics, stable operation, harmless byproducts to the environment, and zero-emission levels with high power and energy density, improved overall performance, and so forth.^{1–5} The performance of the proton exchange membrane fuel cell (PEMFC) is based on the polymer electrolyte membrane (PEM). The Nafion is the vital membrane in PEM. Still, its drawbacks hinder the commercial application due to the deficient durability, low mechanical stability, ion exchange capacity (IEC) and proton conductivity at higher working temperature, fuel crossover, and expensive fabrication. Hence, it is necessary to synthesize a novel polymer electrolyte alternative to Nafion.^{6–9}

The sulfonated aromatic polymers are promising due to the functionalized sulfonic acid group achieving high conduc-

tion.^{10–15} The sulfonated poly(ether sulfone) (SPES) polymer is chosen due to the enhanced proton conductivity, thermo-mechanical stability, easy functionalization, narrow hydrophobic/hydrophilic channels, and good quality film-forming ability at low cost. The sulfone groups and ether linkage of SPES contribute to proton conductivity and chemical stability, while the aromatic group maintains good structural stability. However, SPES possesses low proton conduction at room temperature.^{16–21} Therefore, substantial effort has been made to modify the SPES membrane by fabricating an efficient electrolyte membrane suitable for PEMFC with high proton conductivity and excellent thermo-mechanic stability. Polymers such as sulfonated triazine, sulfonated poly(ether sulfone), and sulfonated poly(ether ether ketone) were fabricated as amorphous porous frameworks, which are attractive designs due to the assembly of nano-cavities that facilitate the proton transfer via the pore channels. The porous structure possesses

Received: March 2, 2022

Revised: May 18, 2022

Published: May 27, 2022



interconnected microstructures that act as the proton transporting channels from one polymer domain to another and afford the continuous proton migration along with the polymer matrix. This porous structure is a promising practical approach for constructing PEM with the tunable porosity and well-interconnected nanostructure; however, the drawback of thermo-mechanical properties is still the primary concern in the porous polymer.^{22–35}

The impregnation of the proton-conducting materials into the pores of the polymer network is a facile method to increase the proton-conducting mechanism through these interconnected porous polymer channels. To achieve better proton conduction with good chemical and thermo-mechanical stability of PEM, the pore filling of an amorphous porous framework by the proton-conducting materials (nano-fillers or ionic liquids or acidic groups) is the effective method. The fabrication of polybenzimidazole with the pore size $\sim 30\text{--}40\ \mu\text{m}$ embedded with polymeric ionic liquid, which fills up these porous structures to facilitate the excellent proton conduction owing to the interconnected proton channels.³⁶ The porous morphology of the [polybenzimidazole and poly(1-vinyl-1,2,4-triazole)] blend membranes uptakes more amount of phosphoric acid (PA) by occupying the porous structure; as a result, it elevates the proton conductivity with lower activation energy as compared to neat PBI.³⁷ The porous membrane with elevated proton conductivity and the thermal property was obtained by introducing the ionic liquid into the blends of polyvinylpyrrolidone and polyimide matrimid via the vapor-induced phase separation method, causing the highly interconnected protonic channels within the porous films.³⁸ In the porous structure, the Nafion membrane achieved superior proton conductivity and excellent stability compared to the non-porous Nafion membrane. Also, the conductivity was stable for more than 4 months at $80\ ^\circ\text{C}$ and 90% RH without any obvious decay.³⁹ The fabrication of porous cross-linked metapolybenzimidazole (*m*-PBI) via the non-solvent-induced phase inversion method exhibits excellent properties such as thermally stable structure with high PA uptake, enriched acid retention and a slight swelling ratio.⁴⁰ The porous membrane of PBI was boosted by the cross-linking method (CpPBI-10) and then doping by PA, which shows the excellent conductivity ($0.046\ \text{S cm}^{-1}$) at $200\ ^\circ\text{C}$ with low water uptake (76.4%).⁴¹ The various proton conducting materials (phosphoric acid, sulfuric acid, triazoles, and imidazole) were introduced into the pores of polymer networks, which briefly shows the crucial proton-conducting mechanisms in the porous polymer matrix and further signifies the novel designing strategies for fuel cell technology.⁴² In this view, we intended to fabricate the amorphous porous framework of SPES (PSPES) for the first time by the simple modified non-solvent-induced phase inversion (MNIPI). After that, the porous structures within the matrix were effectively reinforced by the active proton-conducting filler to enhance the thermo-mechanical stability and proton conductivity via a strong synergistic mechanism.

The 2D hexagonal boron nitrides (BNs) or white graphene analogous to graphite with an equal number of boron (B) and nitrogen (N) atoms arranged in a honeycomb configuration has drawn the attention of researchers over the last decade. The hexagonal phase is more stable among the three BN phases (hexagonal, cubic, and wurtzite). The 2D layers of the BN are bonded by weak van der Waals forces, while the B and N atoms are bonded by the B–N strong covalent bond. The surprising property of BN, when compared to graphene, is its

large surface area, high-temperature anti-oxidation resistance, high chemical resistance, and thermo-mechanical stability.^{43–48} In contrast to BN, the carbon materials contain a black color that makes the polymer nanocomposite opaque. Whereas the BN-based membranes are transparent, the composite can be the preferred color using different fillers. The direct use of hexagonal BN within the polymer matrix faces majorly two challenges. (1) Less interfacial interaction between the hexagonal BN and the polymer matrix. (2) Poor dispersion or aggregation of BN in the polymer matrix leads to weak compatibility. To upsurge the interfacial surface reactivity, the surface modifications on BN are done by incorporating the hydroxyl or alkyl or alkoxy or amide or amine groups.^{49–52}

Thus, the excellent property of hexagonal BN can improve the fuel cell performance on existing PEM by functionalizing the BN surface via active proton conducting groups.^{53–55} The Nafion-incorporated BN and functionalized BNs are utilized as composite PEM for fuel cell application. These show better conductivity with the thermo-mechanical stability due to the hydrogen bond formation between Nafion and hexagonal BN, which is the potential membrane compared to recast Nafion.^{56–58} The 1-pyrenesulfonic acid-functionalized 2D BN nanoflakes and sulfonated BN-incorporated SPEEK were prepared that exhibit the efficient electrolyte membranes with improved durability (diminished chronic edge failure), conductivity, and excellent dimensional stability in contrast to bare SPEEK.^{59,60}

Herein, we synthesis the new amorphous PSPES by impregnating the proton-conducting materials of hydroxylated BN (HBN) within the porous structure of PSPES for the first time via a simple MNIPI. The hydroxyl functionalizations occurred at the electrophilic boron atoms via covalent bonding by the condensation process. The OH groups on hexagonal BN and SO_3H group on PSPES polymer bridging the polymer matrix via functional groups networks ($\text{SO}_3\text{H}\text{--}\text{OH}$) promotes proton pathway channels via Grotthuss and vehicular mechanism. It reinforces the polymer composite matrix via an excellent synergistic effect and increases the thermo-mechanical property. Moreover, we take advantage of porous polymer networks with anchored functionalized filler to achieve suitable mechanical properties with less sacrifice of proton conduction in the PEM for the application of the H_2/O_2 fuel cell.

2. EXPERIMENTAL SECTION

2.1. Materials. Poly(ether sulfone) (PES-Veradel 3000MP) was purchased from Solvay Polymers. Hexagonal BN particles, hydrogen peroxide (30%), chlorosulfonic acid (99% purity), sulfuric acid (98% purity), and *N,N*-dimethylacetamide (anhydrous 99.8% purity) were received from Sigma-Aldrich Chemical Pvt. Ltd. Deionized water was used for the experiments.

2.2. Sulfonation of PES and Functionalization of BN. The sulfonation of PES with the optimized concentration of chlorosulfonic acid and sulfuric acid at room temperature with sufficient time was discussed briefly in our previous literature. The degree of sulfonation $38 \pm 0.03\%$ was confirmed from the ^1H NMR technique by the shift of H_E signal from 7.26 to 8.31 ppm of the hydrogen in the ortho position of the aromatic ring.¹⁹ The NMR signal of SPES such as H_B , H_B' , and H_D (7.26–7.29 ppm) related to the phenyl protons linked with ether and H_A , H_A' , and H_C (7.98–8.1 ppm) are assigned to the phenyl protons linked to the sulfone groups. Moreover, the other NMR signals at 2.51 and 3.91 ppm are attributed to DMSO- d_6 solvent (Figure S1).^{61,62}

HBN was followed by the synthesis procedure of Ivanova et al.⁴⁹ Primarily, the BN was immersed in the hydrogen peroxide ($\text{H}_2\text{O}_2 \sim$

30%, 75 mL) and subjected to ultrasonication for 2 h. Then, the solution was placed in the autoclave at 90 °C for 15 h for better exfoliation and hydroxylation of BN. The exfoliated HBN was centrifuged at 3000 rpm for 30 min to eliminate the bulk sheets. Finally, the exfoliated HBN was obtained after washing with deionized water and dried at 85 °C for 4 h, as depicted in Figure 1a.

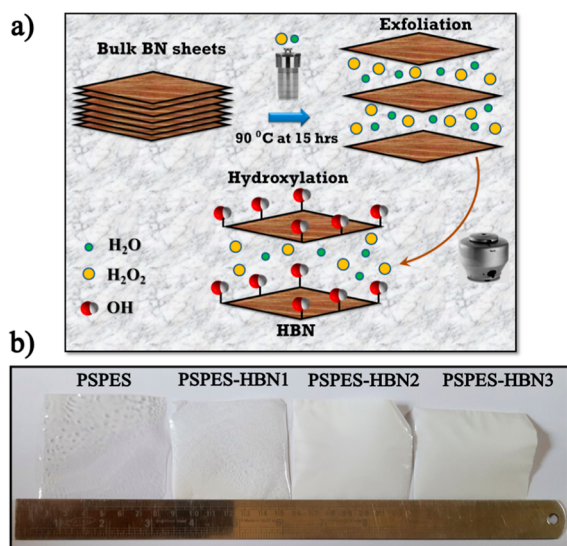


Figure 1. (a) Exfoliation process of HBN and (b) photography of the prepared membranes.

2.3. Preparation of the Amorphous Porous Framework. The preparation of the amorphous PSPES with and without HBN is prepared by the simple MNIPi, followed by the reported works of literature.^{63,64} The desired amount of SPES was added to DMAc solvent and stirred for 4 h. Then, the different amounts of HBN (2, 3.5, and 5 wt %) were dispersed individually in DMAc via the sonication process for 1 h to achieve the homogeneous dispersion of HBN. Finally, these solutions are mixed and stirred for 12 h to afford enough viscous solution to form the composite casting solutions. Then, the solution was poured onto a clean glass plate (10 × 10 cm²), which was placed on a level table and coated using a micrometer precision film applicator. The glass plate was heated at 60 °C to transform into the semiwet or partially evaporated films and then quickly immersed in a water-filled coagulation bath for 12 h to achieve sufficient solvent exchange via phase inversion. Finally, the porous composite membranes with different amounts of HBN (2, 3.5, and 5 wt %) are prepared by removing the glass plate with DI water and dried at 90 °C in a vacuum oven. Hereafter named PSPES-HBN1, PSPES-HBN2, and PSPES-HBN3, as displayed in Figure 1b. The same procedure was followed to prepare the highly porous membrane of SPES (amorphous porous framework) only by using the pure SPES via MNIPi and coded as PSPES. The thickness of the porous membranes varied from 90 to 130 μm prepared via MNIPi and can be folded and bent.

2.4. Characterizations. **2.4.1. Instrumentations.** The XRD study was carried out by the Pro PANalytic instrument using the Cu Kα radiation (λ = 0.154 nm) with a scan range of 10–80°. A PerkinElmer spectrophotometer recorded the Fourier transform infrared (FTIR) spectroscopy measurement from 400 to 4000 cm⁻¹ with a resolution of 4 cm⁻¹. Raman spectroscopy was used to scrutinize the defect sites of BN and HBN by using the RFS27 Bruker device and utilized the Nd:YAG laser (λ = 1064 nm). The samples' morphology and quantitative elemental distribution were observed by field emission scanning electron microscopy (FE-SEM) with energy-dispersive X-ray spectroscopy (EDS) by utilizing Gemini 300, Carl Zeiss instrument with the sputtering of gold. The thermal property of the samples was analyzed from thermogravimetric analysis (TGA) of SDT Q600, TA instruments under a N₂ gas atmosphere with a supply rate of 45 mL

min⁻¹ up to 700 °C. The glass transition temperature (*T_g*) and melting enthalpy (Δ*H_m*) as a function of temperature from 35 to 200 °C were detected by differential scanning calorimetry (DSC) of the same instrument. Before the test, all the samples were heated from room temperature to 120 °C at a heating rate of 10 °C min⁻¹ to remove the excess moisture content. The mechanical property in terms of Young's modulus (MPa), tensile strength (MPa), and elongation at break (%) were determined by a universal testing machine (INSTRON 3365). The sample was 5 × 1 cm² (length × breadth) and was uniaxially stretched at a rate of 2 mm min⁻¹ at room temperature in a dry state.

2.4.2. Measurements. The Fenton test examined the chemical or oxidative stability. The dry-weighted membranes were soaked in Fenton's reagent (2 ppm of FeSO₄ and 3% of H₂O₂) for 12 h at room temperature; measure the degraded weight percentages and rupture time of the membranes. The average standard deviation value was reported from the measurement of three samples of each membrane.

The porosity was evaluated by immersion of the membrane in *n*-butanol for 2 h according to the protocol published.³⁶ The porosity of the membrane was calculated using the following equation

$$\text{porosity (\%)} = \left(\frac{W_B/P_B}{W_M/P_M + W_B/P_B} \right) \times 100 \quad (1)$$

where *W_B* is the amount of absorbed *n*-butanol, *P_B* is the density of *n*-butanol, *W_M* is the weight of the PSPES-HBN membrane, and *P_M* is the density of the membrane.

The water contact angle measurement was done to examine the membrane surface wetting (hydrophilicity) characteristics using a contact angle measuring instrument [Phoenix 300 Touch, SEO Surface Electro Optics]. The contact angle was measured using deionized water as probe liquid at three random places of the membrane, and the average standard deviation value was reported.

The dimensional changes concerning water uptake and swelling ratio were measured by the increase/decrease in weight (g) and thickness (cm²) of the dry samples (*W_{dry}* and *T_{dry}*) after soaking in deionized water for 24 h at predetermined temperatures (30–80 °C). Over time, water absorption was assessed for the wet membranes by weighing again (*W_{wet}* and *T_{wet}*). The following equation evaluates the water uptake and swelling ratio from the observed values

$$\text{change in weight (\%)} = \left(\frac{W_{\text{wet}} - W_{\text{dry}}}{W_{\text{dry}}} \right) \times 100 \quad (2)$$

$$\text{change in thickness (\%)} = \left(\frac{T_{\text{wet}} - T_{\text{dry}}}{T_{\text{dry}}} \right) \times 100 \quad (3)$$

A standard acid–base titration measures the IEC. In brief, the vacuum-dried membranes were transferred into the 0.1 M NaCl solution and soaked for 24 h to exchange Na⁺ ions in the solution with H⁺ ions in the membrane. Then, the solution was titrated against 0.01 NaOH base solution using phenolphthalein as an indicator, and the IEC (mequiv g⁻¹) was calculated using the following relation.

$$\begin{aligned} \text{Ion exchange capacity (mequiv g}^{-1}\text{)} \\ = \left(\frac{\text{volume} \times \text{normality}}{\text{dry weight of polymer membrane}} \right) \end{aligned} \quad (4)$$

where volume and normality are taken for NaOH.

The hydration number (λ) assists the number of water molecules absorbed per one functional group of sulfonic acid and is calculated using eq 5

$$\lambda = \left(\frac{\text{water uptake}}{\text{molecular weight of water}} \right) \left(\frac{10}{\text{IEC}} \right) \quad (5)$$

The proton conductivity of PSPES and PSPES-HBN membranes was measured by the AC impedance spectroscopic method via the potentiostat/galvanostat Squidstat Plus analyzer of Admiral Instru-

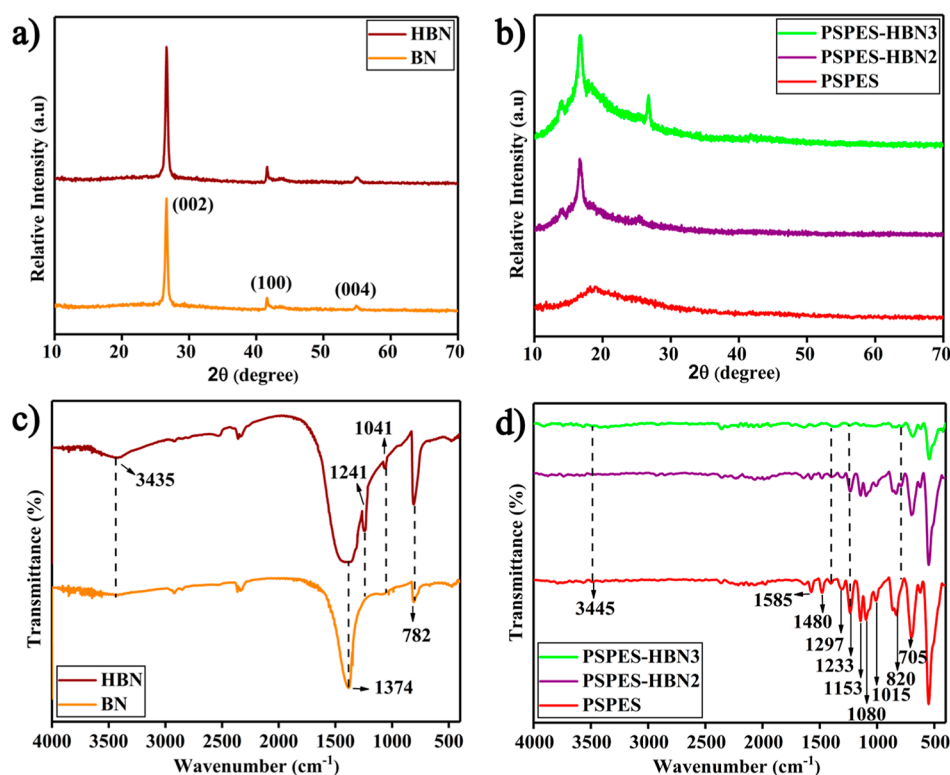


Figure 2. (a) XRD and (c) FTIR patterns of BN and HBN, and (b) XRD and (d) FTIR patterns of the PSPES, PSPES-HBN2, and PSPES-HBN3 membranes.

ments, USA. Before the test, all the membranes were dried in a vacuum oven for 12 h; afterward, these membranes were inserted between the two stainless steel disc electrodes (20 mm diameter) under fully humidified conditions. The frequency response analyzer of Squidstat Plus with the thermo-controlled cell (range from 30 to 80 °C) and sweeping the frequencies from 10 MHz to 10 Hz at a fixed scan rate of 10 mV in the 100% relative humidity (RH) were used for investigation. The humidification condition during measurement was maintained by using the humidity setup. The distances between the electrodes or membrane thickness (L , mm), cross-sectional area (A , cm²), and bulk resistance (R , Ω) were measured to determine the proton conductivity (σ , S cm⁻¹) of the membranes using eq 6. The measurements were repeated thrice for each sample, and the average standard deviation values were reported as the reproducibility results.

$$\sigma \text{ (S cm}^{-1}\text{)} = \frac{L}{(R \times A)} \quad (6)$$

The activation energy (E_a) was calculated from the slope of the proton conductivity Nyquist plot against the temperature using the Arrhenius equation.

$$\text{Ln}(\sigma) = \text{Ln}(\sigma_0) - \left(\frac{E_a}{RT} \right) \quad (7)$$

where σ and σ_0 are the proton conductivity (mS cm⁻¹) and the pre-exponential factor (mS K⁻¹ cm⁻¹), and E_a , R , and T are the activation energy (kJ mol⁻¹), universal gas constant (8.314 J mol⁻¹ K⁻¹), and absolute temperature (K).

The single-cell test for H₂/O₂ fuel cell performance was evaluated in Bio-Logic Science Instrument, as described in our previous literature.¹³ In brief, the anode and cathode section comprises a gas diffusion layer with commercial carbon cloth, coated with the catalyst ink (a mixture of Pt/C, Nafion, doubly distilled water, and isopropyl alcohol with the required amount) via spraying technique. The MEA was equipped by stacking the electrolyte membranes between the as prepared GDL electrodes through a hot pressing technique at 125 °C with 2 psi for 1 min. Afterward, the MEA single-cell fixture was

airtight sealed along with the bipolar graphite plates with a serpentine flow channel. The test was evaluated with the active cell area of 5 cm² at the cell temperature of 80 °C at 100% RH with the fixed fuel and oxidant flow rates of 250 and 500 ccm under 2 psi pressure. Before the measurement, the cell was maintained at 60 °C for 2 h and tested for five on-off cycles, each of about 25 min at high power density. Then, the above condition was reset to 80 °C with 100% RH and activated the cell with the varying galvanostatic current mode to measure the cell voltage and power density. The continuous durability test was performed at a constant loading current of 0.2 A cm⁻² at 80 °C for 120 h with the same condition as cell performance.

3. RESULTS AND DISCUSSION

The XRD patterns of BN, HBN, PSPES, and its composite membranes are shown in Figure 2a,b. The BN exhibits low intense peaks at 26.16 (002), 41.56 (100), and 54.81 (004) as compared to HBN due to the attachment of the hydroxyl (OH) group on the edges of BN sheets. However, the crystalline nature is not destroyed by the hydroxylation treatment. This causes the re-orientation and restacking of sheets, altering the scattering parameters and producing intense high peaks.⁶⁵ The pure PSPES shows its amorphous nature with a broad halo peak at 2θ of 18.15°. The impregnation of HBN (3.5 and 5 wt %) into the porous matrix alters the crystallinity of PSPES-HBN2 by forming a strong interfacial bond between the OH of BN and SO₃H of PSPES. This reduced the intensity of the PSPES-HBN2 membrane compared to the PSPES-HBN3 membrane because the good interfacial interplay between the HBN and PSPES occurred only at 3.5 wt % of HBN in the porous matrix of PSPES. Although 5 wt % of HBN tends to induce bad interfacial interplays in the PSPES in the results, the aggregate effect was observed. Thus, the high dispersion ability of HBN to create the amorphous phase in the PSPES-HBN2 membrane may be

effective for upgrading the proton conductivity of the PSPES-HBN membrane.⁶⁷

Figure 2c,d displays the FTIR spectrum of BN, HBN, PSPES, and its composite membranes. The vibration peaks at 782 and 1374 cm^{-1} correspond to the B–N–B bond's out-plane and in-plane vibrations in BN sheets. The appearance of highly intense and new peaks at 3435, 1241, and 1041 cm^{-1} are assigned to O–H, B–OH, and B–O bonds of HBN, which confirms the formation of HBN via hydroxylation of BN (Figure 2c).^{44,68,69} The successful sulfonation of PES was prominently identified by the 3445, 1015, and 1080 cm^{-1} peaks for the OH vibration, symmetric and asymmetric stretching modes of the SO_3H group. The SO_3^- vibrations of the sulfonic acid groups are presented at 1297 and 1233 cm^{-1} , respectively. The sulfone group's symmetry and asymmetric stretching peaks are found at 1153 cm^{-1} . The peaks at 1480 and 1585 cm^{-1} correspond to the C=C stretching vibration of the aromatic groups. The peaks at 705 and 820 cm^{-1} are related to the C–S and S–O vibration, signifying the presence of sulfonic acid in PSPES.^{13,67,70} In the PSPES-HBN porous structure, the SO_3H group of PSPES interacts strongly with the OH groups on the hexagonal ring of HBN dispersed within the matrix. The composite membranes of PSPES-HBN2 and PSPES-HBN3 contained all the peaks of each component of HBN and PSPES. The less intensified peaks of sulfonic acid (1080, 1153, 1297, and 1233 cm^{-1}) in the PSPES-HBN composite membranes compared with PSPES reveal the excellent compatibility between the PSPES and HBN via SO_3H with the OH group.

Figure S2 illustrates the Raman spectrum of the BN and HBN. At first, for the bulk BN, the Raman peak appears at 1365 cm^{-1} , revealing a characteristic peak corresponding to the phonon mode (E_{2g} mode). Following the exfoliation process, the result was established in the phonon mode at 1367 cm^{-1} , with a shift of 2 cm^{-1} . This phenomenon details the expansion of the B–N bonds in BN due to the interlayer interplay that causes the softening of the phonon modes compared to monolayer HBN. In contrast, the interlayer interactions are absent in HBN and cause the shortened B–N. This difference in phonon frequency shows the formation of few-layered HBN sheets.⁷¹

From the FE-SEM analysis, the BN reveals a more stacked morphology (Figure 3a,b) as compared to the HBN (Figure 3c,d) due to the presence of van der Waals force between the

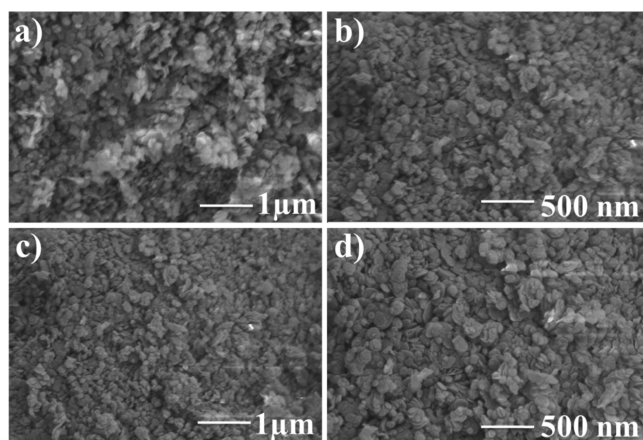


Figure 3. FE-SEM images of (a,b) BN and (c,d) HBN.

individual sheets, whereas it was lessened in the HBN sheets. The exfoliation process drove this and further increased hydroxylation due to the occupation of OH at the edges of these sheets, which caused them to separate the individual sheets from stacking.⁶⁵ Figure S3a,b shows the elemental mapping images that distinguish the formation of HBN from BN via exfoliation and hydroxylation, which further validated the elemental distribution of oxygen in HBN as compared to BN.

The necessary macroscopic properties, including mechanical strength, water uptake, proton conductivity, and durability, are significantly influenced by the inner morphology and the dispersion of the filler in composite membranes. The surface and cross-sectional FE-SEM images of PSPES, PSPES-HBN1, PSPES-HBN2, and PSPES-HBN3 membranes are shown in Figures 4a–d, 5a–f, and 5Sa–d, respectively. As seen in the

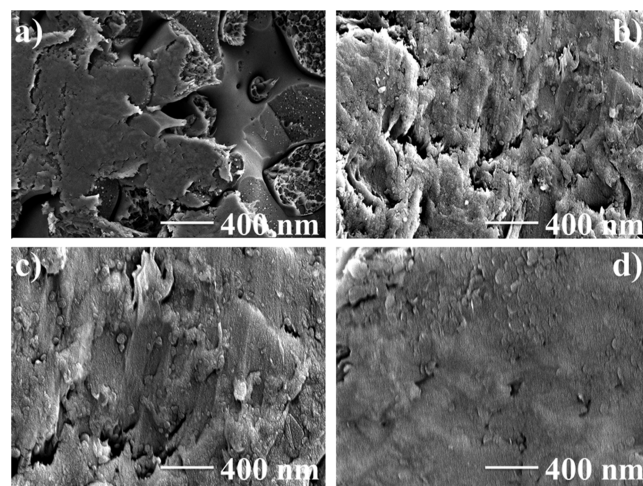


Figure 4. Surface FE-SEM images of (a) PSPES, (b) PSPES-HBN1, (c) PSPES-HBN2, and (d) PSPES-HBN3 membranes.

cross-section and surface images, all the membranes exhibit small pore openings in the matrix. The surface images in Figure 4a–d point out the presence of underlying open pores, which is understood by magnifying the surfaces with tiny pores. This is favorable for the membrane's efficient fuel cell performance and reduces stability.⁴⁰

As seen in Figures 5b–d and 5Sb–d, a porous matrix structure is created for all phase inverted PSPES membranes amid the even distribution of both small and medium pores not as large. The entire cross-section FE-SEM images of PSPES-HBN composite membranes exhibits the dense circular micro-porous structures, but the pure PSPES membrane shows a highly porous structure (Figures 5a and 5Sa). In addition, the PSPES-HBN membranes with the increase in HBN content illustrate that the HBN particles can also achieve a uniform dispersion with regular shapes and sizes with HBN up to 3.5 wt %. Further study of the high magnification FE-SEM image of the PSPES-HBN2 (Figure 5e,f) reveals the dense outer surface with hierarchical micro-pores structure and consequently attaches the HBN tightly to the matrix.

Moreover, as the HBN content increases, more particles are anchored into the micro-porous instead of being removed from the matrix, indicating the strong bond at the HBN-PSPES interfaces.²⁵ The pore size of PSPES-HBN varies at <300 nm, with spherical shapes exhibiting low porosities and less interconnected structures. At the same time, the PSPES

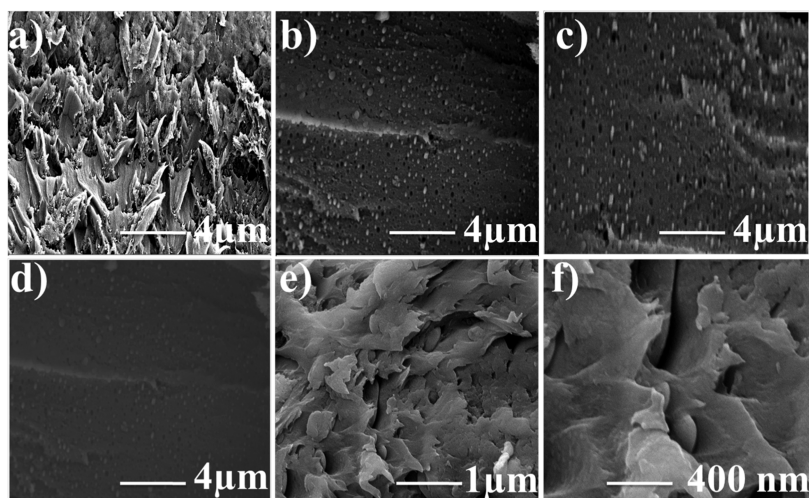


Figure 5. Cross-sectional FE-SEM images of (a) PSPES, (b) PSPES-HBN1, (c,e,f) PSPES-HBN2, and (d) PSPES-HBN3 membranes.

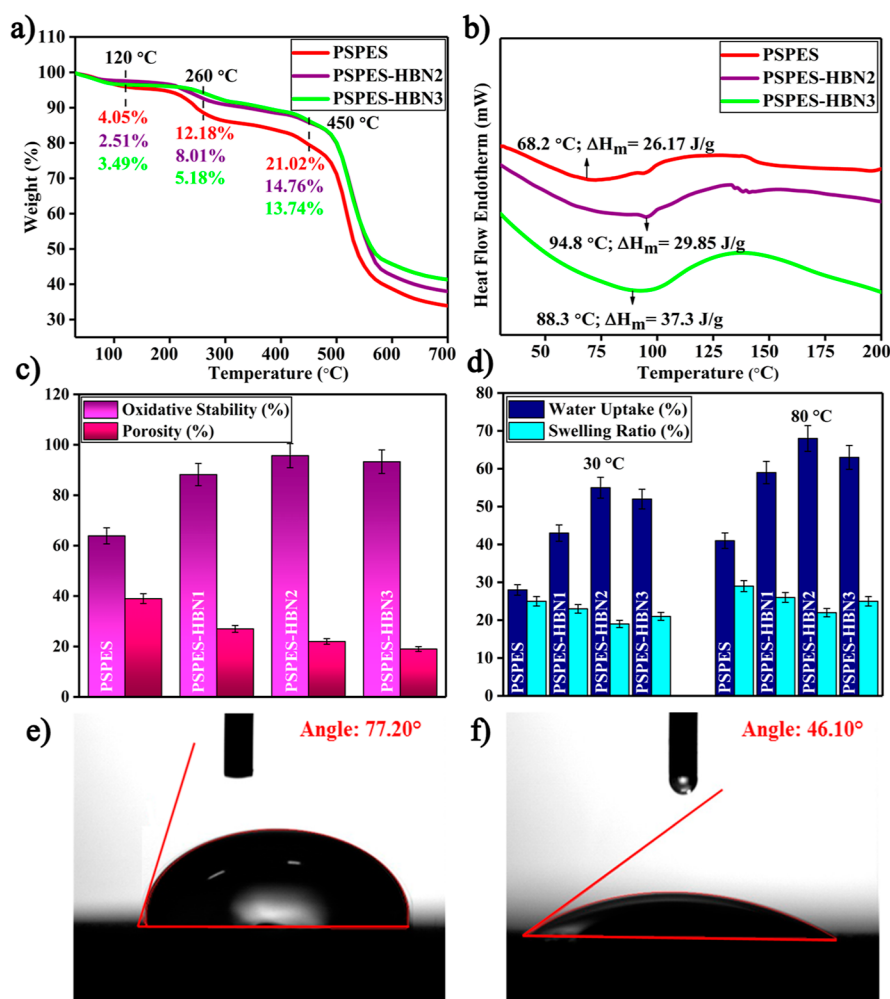


Figure 6. (a) TGA, (b) DCS, (c) oxidative stability with porosity, (d) water uptake with the swelling ratio for PSPES and PSPES-HBN composite membranes, and water contact angle for (e) PSPES and (f) PSPES-HBN2 membranes.

membrane with a pore size of 1–2 μm and a very irregular shape shows a high porosity level and high interconnected structures. Additionally, filling up all these micro-pores can reduce the quantity of fuel cross-over, which is the main problem of MEA tests in PEMFC. It might lead to high gas

cross-over and decrease the performance and durability or cause instant failure during preliminary testing.⁷²

The uniform dispersion and good interaction of HBN particles validate better compatibility and tight interfacial contact between the HBN and PSPES via functional groups of hydroxyl and sulfonic acids within the porous structure.

Table 1. Comparison Table of Mechanical Properties of the PSPES-HBN Composite Membrane

membrane codes	Young's modulus (MPa)	tensile strength (MPa)	elongation at break (%)	porosity (%)	references
SPES	1248 ± 62	12.3 ± 0.6	29.4 ± 1.4		13
PSPES	653.3 ± 0.2	11.7 ± 0.4	17.93 ± 0.9	37 ± 1.95	this work
PSPES-HBN1	890 ± 0.9	15.9 ± 0.7	10.4 ± 0.3	27 ± 1.35	this work
PSPES-HBN2	1018.1 ± 0.5	17.7 ± 0.1	7.88 ± 0.8	22 ± 1.1	this work
PSPES-HBN3	931.5 ± 0.8	16.8 ± 0.5	5.64 ± 0.7	19 ± 0.95	this work
mp-50		3.69		47	26
P-25 μm	0.2 ± 0.02	0.9 ± 0.7		42.5	36
P-25 μm-0% CL	0.9 ± 0.04	2.5 ± 0.5			36
pPBI-10	40.17	3.33	31.25	34.01	41
CpPBI-10	151.48	10.17	53.64	24.47	41
M1-P	33.34 ± 2.02	0.867 ± 0.01		45.45 ± 1.45	63
M2-S	28.45 ± 1.75	0.496 ± 0.7		30.42 ± 2.40	63
M3-C	45.63 ± 1.60	0.872 ± 0.05		60.26 ± 2.46	63
porous PBI		11.5	11.2		81
acid doped PBI		6.8	192		81
pPBI-33	0.63 GPa	~72		28.7	82
CpPBI-60	0.9 GPa	82.9		37.8	82

However, some aggregation effect was found in the PSPES-HBN3 due to the less dispersive ability of HBN (5 wt %) in the PSPES matrix, which clearly shows the irregular shape of HBN with a broader size in the surface FE-SEM image (Figures 5d and S5d) and further confirmed in the elemental mapping results of the PSPES composite membranes (Figure S4a–c). This proves the poor compatibility and weak interfacial contact between the HBN and PSPES, as shown in Figure S4c, and the excellent dispersion ability of HBN was observed in PSPES-HBN1 and PSPES-HBN2 of Figure S4a,b. The HBN reinforcement enables the formation of the dense porous structure of PSPES without any defect, which is beneficial for the selective permeation of protons (H⁺) more willingly than fuel molecules and enhances mechanical, thermal strength, and oxidative stability of the PSPES membrane.²³

The degradation and deformation of membranes in terms of temperature were evaluated by the TGA and DSC analysis. The TGA thermographs of the porous structured membranes are displayed in Figure 6a. All the porous membranes exhibited the similar sort of three-stage degradation patterns: (1) <110 °C owing to the evaporation of water molecule, (2) around 220 °C related to the SO₃H group decay from the backbone of the polymer, and (3) above 450 °C attributed to the decomposition of the aromatic polymer chain. The PSPES membrane exhibited 12.18 and 21.02% weight loss at 260 and 450 °C. Compared to the pristine PSPES membrane, all the PSPES-HBN composite membranes exhibited retarded degradation. However, the PSPES-HBN2 membrane revealed weight losses of 8.01 and 14.76 at 260 and 450 °C. The inflated thermal stability endorsed the tortuous path effect and radical scavenging ability of HBN, which slows down the discharge of volatile products and hinders the heat transport.^{49,73} Also, the decomposition of HBN inside the pores of the PSPES takes a wider temperature range of 280–450 °C and thus reduces the decomposition and segmental motion in contrast to PSPES.⁵⁷ The strong interfacial interaction between the OH group of HBN and SO₃H group of PSPES matrix prohibits the movement of polymer chains, already evidenced from the FTIR analysis. The PSPES-HBN2 membrane is relatively stable up to 550 °C, which is superior to their working temperatures in fuel cells. The weight loss of the PSPES-HBN2 membrane is less than that of PSPES and SPES

because the incorporation of HBN in PSPES increases the interaction between HBN and PSPES that effectively constrains the polymer movement against the thermal degradation of the PSPES polymer matrix as the casted SPES membrane exhibited 11.39 and 20.48% weight losses at 260 and 450 °C.¹³ Overall, the well-designed porous structure's thermal stabilities and the impregnation of uniformly distributed HBN endowed the better operating temperature of PEMFC.

The chain packaging and mobility of the membrane are further studied by DSC analysis in Figure 6b. The glass transition temperature (T_g) and melting enthalpy (ΔH_m) were observed for the PSPES and PSPES-HBN composite membranes. The combination of PSPES with HBN increased the T_g value due to the strong interaction between the SO₃H group of PSPES and the OH group of HBN at the polymer–filler interface of the porous framework. Moreover, the chain mobility of PSPES was suppressed by impregnating HBN into pores, thus improving the T_g . The OH groups at the edges of HBN cause lesser interfacial contact between the sheets, paving the way for its uniform dispersion and forming less crystallized matrices. The ionic interaction of PSPES and HBN greatly hinders the re-orientation of crystalline domains and reduces the polymer matrices' crystallinity. The PSPES-HBN2 and PSPES-HBN3 membranes display the enhanced T_g value of 94.8 and 88.3 °C. The T_g of all the PSPES-HBN membranes is higher than that of the PSPES (68.2 °C) and SPES (71.8 °C) owing to the filling up the PSPES matrix with HBN causes higher interaction between HBN and PSPES, which significantly controls the polymer domain motion between the adjacent matrix leading to the alternation of the macrostructure structure.¹³ Also, the membrane's melting enthalpy (ΔH_m) increases with the increase of HBN in the PSPES matrix, which affords the rigidity of the polymer chain package. This property provided enhanced and favorable conditions for fuel cell conditions.

Strong durability and chemical stability of the membrane are of great significance for the fuel cell performance and the lifetime of PEMFC.^{74–78} The oxidative stability of PSPES membranes was measured by immersing the membrane in Fenton's reagent at room temperature. The results were displayed in Figure 6c, which shows the degradation of the

membranes that depends on the porosity and HBN incorporation.²³ The PSPES started to fracture after 12 h and revealed $63.95 \pm 3.19\%$ of weight retention at 12 h. The porous nature of the PSPES matrix exhibits a higher surface area. It creates the chances for the higher interaction of free radicals with the polymer functional groups (sulfonic acid), which may initiate the chain degradation or dissociation and causes higher weight loss. The weight retention of the casted non-porous SPES membrane is $80.12 \pm 4.3\%$ which is higher than the PSPES membrane due to the absence of porosity in the membrane.¹³ However, the reinforcement of HBN into the PSPES membrane exhibits higher weight retention due to strong interfacial interplay between HBN and PSPES that preserves the polymer functional groups. The weight retention of PSPES-HBN composite membranes is higher (88.2 ± 4.41 , 95.7 ± 4.78 , and $93.9 \pm 4.66\%$), and all the fracture time is above 16 h with the increase in HBN contents from 2 to 5 wt % due to its dense porous nature and its impregnation by HBN.^{24,79} These made the physical cross-linking network structure of the PSPES membrane through strong interaction between the PSPES and HBN at the $\text{SO}_3\text{H}-\text{OH}$ interface, which probably caused the polymer chain to be less attacked by radical species and enhanced the oxidative stability.¹⁵

To analyze the porous nature of the PSPES membranes, the porosity test was performed using *n*-butanol as an adsorbing source, as displayed in Figure 6c. The PSPES membranes synthesized through the MNIPi method had a high porosity, around $39 \pm 1.95\%$. The porosity values of PSPES-HBN composite membranes also decrease with the increase in the HBN concentration in PSPES, probably due to densification of the membrane (dense porous structure) from the strong interaction of PSPES with HBN with the occupation of HBN in the porous site of the membrane.⁷⁹ Yet, the HBN incorporation influences the porosity is insignificant and does not affect the porosity value.

The mechanical property of the PSPES membranes was evaluated and detected that the impregnation of HBN into the porous structure of SPES improves the tensile strength, as verified in Table 1. The PSPES-HBN2 composite membrane displayed a tensile strength of 17.7 ± 0.1 MPa with Young's modulus of 1018.1 ± 0.5 MPa and elongation break at $7.88 \pm 0.8\%$. In contrast, the pristine PSPES membrane possessed a tensile strength of 14.7 ± 0.4 MPa with Young's modulus of 653.3 ± 0.2 MPa and elongation break at $17.93 \pm 0.9\%$. About 1.2 and 1.5% increment in the tensile strength and Young's modulus of the PSPES-HBN2 composite membrane is mainly due to the lessened phase separation owing to the result of even dispersion of HBN and the porous structure PSPES. The incorporation of HBN into the PSPES matrix produced the uniform distribution along with the polymer matrix and into pores induces the strong interfacial interplay between PSPES and HBN to trigger the reinforcement effect of the PSPES polymer matrix by using this synergetic effect. The OH groups at the edges of BN firmly form an interfacial interaction with the SO_3H group of PSPES, making the membrane more rigid and changing its nature from ductile to brittle. However, with the excessive addition of HBN (5 wt %), it is seen that tensile strength becomes lower than other PSPES-HBN composite membranes. It may be associated with the poor dispersion and weak interplay of excess HBN in the porous structure, as verified from EDS analysis.^{50,80} Also, the tensile strength of the PSPES-HBN2 membrane is more significant than cast SPES (12.3 ± 0.6 MPa)¹³ with a dense structure when compared

with PSPES (11.7 ± 0.4 MPa) structure as the PSPES exhibits a low value due to the porous structure. Consequently, the porous PSPES-HBN composite membranes fabricated in this work show better functional mechanical integrity than other porous membranes sustainable for PEMFC operations from the comparison in Table 1.

The water contact angle was calculated to estimate the change in the hydrophilic property of PSPES and its composite membrane (PSPES-HBN2). The effect of the addition of HBN sheets on the PSPES with its synergy interaction along with the porosity and membrane roughness was observed from the water contact angle. When the concentration of HBN in PSPES casting solution is 3.5 wt %, the water contact angle of the PSPES membrane is decreased. As shown in Figure 6e,f, the water contact angle of the PSPES membrane was 77.20, which is higher than the PSPES-HBN2 membrane (46.10) due to the wide and interconnected hydrophilic domains that promote the water contact with the membrane. The introduced HBN sheets reduced the water contact angle of PSPES membranes significantly, indicating a more hydrophilic surface that contains more water-reactive polar OH groups than PSPES.^{83–85}

The water uptake is a vital parameter that governs the membrane performance, which was analyzed for all the PSPES membranes and compared with Nafion-117. As the ideal PEM must absorb and retain more water and lower swelling, the water uptake and swelling ratio were examined with the temperature rising from 30 to 80 °C in Figure 6d. The porous nature holds more water molecules within the PSPES matrix than SPES due to the occupation of water molecules in the porous structure and its higher surface area, inducing the interaction between H_2O and SO_3H , leading to a high water uptake value. The PSPES-HBN membrane significantly improves the water uptake than the SPES and PSPES by effectively using the HBN content via a synergistic effect between the HBN and SO_3H . Specifically, at 80 °C, the water uptake of PSPES possesses $41 \pm 2.05\%$. However, the PSPES-HBN1, PSPES-HBN2, and PSPES-HBN3 membranes observed water uptakes of 59 ± 2.95 , 68 ± 3.4 , and $63 \pm 3.15\%$, respectively. With the impregnation of HBN into the porous networks of PSPES, the water uptake increases due to the hydrophilicity of HBN and the sulfone groups of PSPES. The only possible reason is the proper dispersion of HBN particles within the amorphous porous framework of PSPES, which generates an excess number of active sites at the polymer–filler interface to the hold water molecule through the functional group SO_3H and OH.^{16,21} Consequently, the hydrophilic nature was augmented, plus the hydrophilicity of the high-density sulfonic acid within the amorphous porous network. Also, the porous membranes possess a permanent pore structure, which affords the proton transfer channel through the ionic cluster. With the introduction of 3.5 wt % of HBN in the PSPES matrix, the water uptake of $68 \pm 3.4\%$ was obtained, higher than that of the commercial Nafion-117 membrane ($32.5 \pm 0.9\%$).⁸⁶ The temperature-dependent water uptake of PSPES-HBN membranes increases with the HBN content, but the water uptakes decrease at 5 wt % owing to the aggregation of HBN.

Figure 6d shows the swelling that occurred in membranes after water uptake at the temperatures of 30 and 80 °C. The swelling ratio of the PSPES-HBN composite membranes demonstrates the inverse behavior to that of water uptake. The 2D structure of HBN contains the OH group afforded the

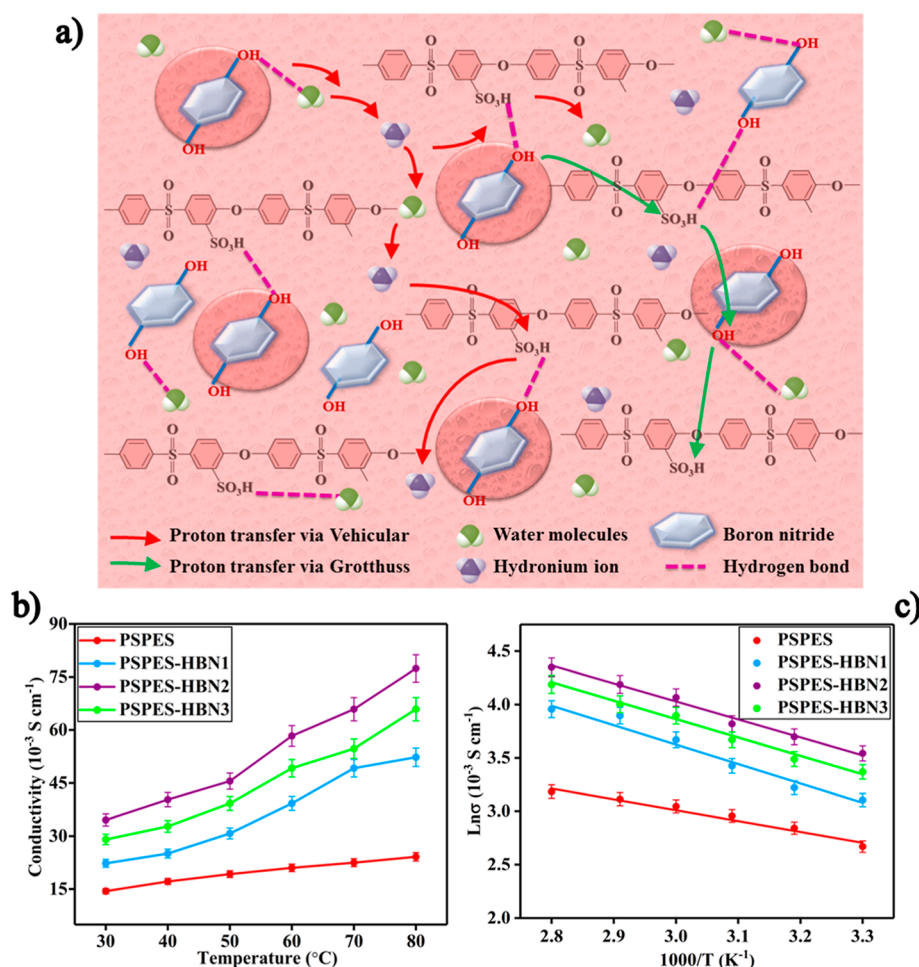


Figure 7. (a) Schematic representation of proton conduction mechanism along with (b) proton conductivity and (c) Arrhenius plot of the prepared porous membrane.

more vital interfacial interaction with the SO₃H group of PSPES, which reinforces the porous composite matrix and designs the well compact structure that prevents the swelling. The exceptional reduced swelling ratio of PSPES-HBN2 is $22 \pm 1.1\%$ which could be attributed to the amorphous porous framework's inherent mechanical stability, which is lower than the commercial Nafion-117 membrane ($25.1 \pm 0.9\%$).⁸⁶ The hydrophilic backbone (OH) creates a more vital interfacial interaction with the SO₃H groups, prevents much swelling effectively, and forms a more compact structure of composite membranes, consistent with the results from SEM.^{17,50,87}

IEC governs the exchangeable proton capacity in PSPES membranes, detected from the standard acid-base titration method. As collected from the results, the pure PSPES membrane showed the IEC value of 1.58 ± 0.01 mequiv g⁻¹. The incremental incorporation of HBN in the PSPES membrane underwent much higher IEC. The PSPES-HBN1, PSPES-HBN2, and PSPES-HBN3 give the IEC values of 1.69 ± 0.01 , 1.89 ± 0.01 , and 1.77 ± 0.01 mequiv g⁻¹, respectively. Also, the PSPES and PSPES-HBN composites manifest higher IEC than Nafion-117 (0.91 ± 0.01 mequiv g⁻¹).⁸⁶ In the PSPES-HBN2 composite membrane, a slight increment IEC value suggests that the 3.5 wt % HBN in the porous amorphous framework of PSPES can improve the concentration of conducting protons. These are owing to the strong interaction between HBN and SPES via hydroxyl and sulfonic

acids groups that provide the more conducting channels. The lower IEC value of the PSPES-HBN3 membrane (1.77 mequiv g⁻¹) may be due to the scarcity of exchangeable Na⁺ ions during titration, which may be due to the lack of SO₃H groups. It is noteworthy to mention that adequate ionic sites on the surface of HBN and PSPES subsequently increase the per cluster volume of ionic sites in the PSPES-HBN matrix, which increases the IEC.^{67,88}

The hydration number (λ) is also linear with water uptake and the IEC parameter. The PSPES-HBN2 composite membrane showed the maximum λ value of 19.94, associated with more bound water molecules gathering around the hydrophilic sulfonic acid and hydroxyl group via the strong ionic interaction with the HBN and PSPES.⁸⁹ The enhanced λ value of the PSPES-HBN composite membranes is associated with higher water uptakes, which bring more possibility for vehicle-type proton conduction in the PSPES composite membranes. The λ value for PSPES, PSPES-HBN1, PSPES-HBN2, and PSPES-HBN3 membranes are 14.36, 19.34, 19.94, and 19.71. The PSPES-HBN2 composite membrane exhibited a higher λ value than the Nafion-117 membrane of 19.2.⁸⁶

Integrating HBN in the PSPES matrix improves the water uptake, swelling ratio, and hydration number, directly influencing the proton conductivity. Figure 7b shows the proton conductivities of pristine PEPES and PSPES-HBN composites at various temperatures (30–80 °C) with 100%

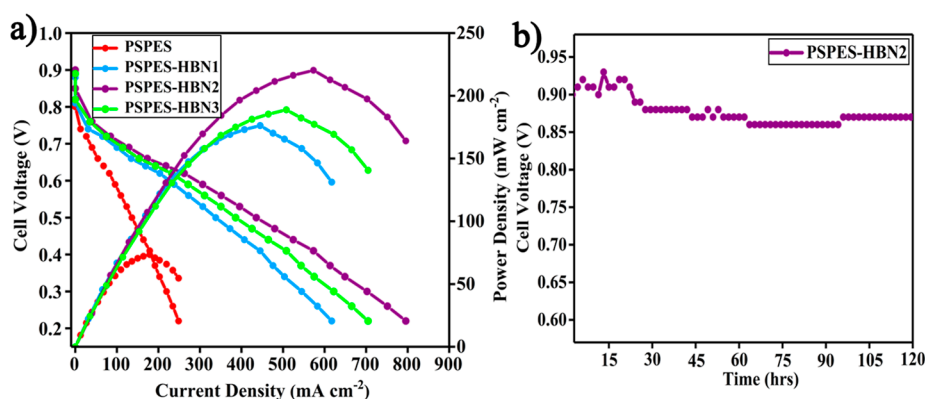


Figure 8. (a) Polarization curves for all the membranes and (b) accelerated durability test operation for the PSPES-HBN2 membranes in 120 h at 80 °C.

RH. The PSPES-HBN composite membranes revealed higher proton conductivity than PSPES ($14.43 \pm 0.7 \text{ mS cm}^{-1}$) and non-porous casted SPES ($11.74 \pm 0.58 \text{ mS cm}^{-1}$) at 30 °C with 100% RH.¹³ Moreover, the PSPES membrane exhibited more conductivity than the non-porous casted SPES facilitated by the porous proton pathways channels and higher active surface area, triggering the enhanced conduction mechanism in terms of vehicular and Grotthuss. The amorphous porous network successfully designed the hydrophilic structure and high-density sulfonic acid units. These PSPES membranes also possess an enduring pores structural framework (highly porous nature), which affords a proton transport channel along with the PSPES polymer matrix.²² However, the proton conductivity of PSPES-HBN tends to increase by incorporating various amounts of HBN into the PSPES matrix due to the formation of the dense pore structure. This phenomenon can be credited solely to the HBN and its synergistic effect with PSPES. It acts as a transport medium and crucial element in the proton conducting mechanism, which interconnects ion-conducting channels in the PSPES matrix. Generally, proton transport occurs in two mechanisms: (i) Grotthuss and (ii) vehicular, schematically represented in Figure 7a. At 30 °C, the vehicular mechanism dominates the proton diffuses with H_3O^+ ions and increases proton mobility, which points the membrane's molecular diffusion. At 80 °C, the Grotthuss dominates the molecular diffusion owing to the lack of water content in the membrane, augmenting the proton mobility and leading to structural diffusion.⁹⁰ The use of sulfonic acid-containing units in the PSPES polymer (highly porous) combined with HBN containing many hydroxyl groups within a hierarchical porous organic framework may enhance the higher interfacial interplay between HBN and PSPES via OH and SO_3H . It favors the proton transport mechanism in vehicular and Grotthuss types by using BN's active functional groups and inherent conducting property (H^+).⁵⁰ The interaction of boron atoms (B^+) with protons (H_3O^+) leads to favor the vehicular mechanism, and the size of its high pores with a minimized potential barrier at the center of hexagonal rings induced the proton transport through HBN sheets.⁸⁶

Furthermore, by impregnating HBN into the porous framework of PSPES, they are permanently caged inside the pores, yielding excellent OH retention ability by interacting with the SO_3H of PSPES. At the same time, OH groups may lead to the formation of hydroxyl domains with sulfonic acid ($\text{SO}_3\text{H}-\text{OH}$) in the porous structure to transfer protons that obeyed the Grotthuss mechanism.²⁶ It can facilitate higher

proton conductivity than the PSPES at lower and higher operating temperatures. Under identical conditions, the proton conductivity of the PSPES-HBN2 membrane was $77.4 \pm 3.87 \text{ mS cm}^{-1}$, which was 3.2 times as much as the pure PSPES. The aggregation effect of fillers appeared in PSPES-HBN3 due to the excess amount of HBN in PSPES that blocks the proton movement. The results decrease the proton conductivity of the PSPES-HBN3 membrane ($65.9 \pm 3.29 \text{ mS cm}^{-1}$) compared to the PSPES-HBN2 membrane ($77.4 \pm 3.87 \text{ mS cm}^{-1}$). Also, the PSPES-HBN composite membrane discloses higher proton conductivity than the commercial Nafion-117 membrane of 26 mS cm^{-1} .⁴⁷ Proton conductivities of all PEMs increased as the temperature increased from 30 to 80 °C because of the rapid proton mobility via polymer ionic channels with minimized energy barriers.

Arrhenius-type proton conductivity was exploited to calculate the activation energy (E_a) (Figure 7c), which refers to the minimum energy required for proton transport from one site to the nearer site. The E_a of PSPES was $11.67 \pm 0.5 \text{ kJ mol}^{-1}$, and the PSPES-HBN composites showed lower values of 9.28 ± 0.4 , 8.55 ± 0.4 to $7.36 \pm 0.3 \text{ kJ mol}^{-1}$, indicating that the proton conduction is preceded via the vehicular and Grotthuss mechanism but predominantly vehicular owing to the activation energy of sulfonated polymers.^{16,90} The PSPES-HBN2 membrane displays a lower E_a value than Nafion-117 of $14.1 \pm 0.4 \text{ kJ mol}^{-1}$.⁸⁶

Considering the significance of applicability in PEMFCs and the excellent proton conductivity of the membranes, the PEMs were subjected to a single-cell polarization test at 80 °C with 100% RH at ambient pressure, which is demonstrated in Figure 8a. PEMFCs promise alternative power delivery systems due to their high energy efficiency. However, our method for synthesizing an amorphous porous polymer reported herein is very simple, involving inexpensive reagents under convenient refluxing conditions. Because the sulfonic acid-containing organic matrix was used to synthesize this amorphous proton conductive organic framework with abundant porosity, the high mobility of protons inside the pore channels can be achieved. This phenomenon may result from sharply enhanced proton diffusion in the larger pores and interconnected membrane pores at elevated temperatures.^{25,36} After incorporating HBN, the dense pore structures are created, and HBN ultimately anchors the pore regions with the evenly distributed HBN layers found on the PSPES matrix. These are adequate to serve as a proton diffusion path between the HBN and PSPES by using functional groups of OH and SO_3H , which

Table 2. Comparison of Porous Structured Membranes

membrane codes	temperature (°C)	proton conductivity (mS cm ⁻¹)	power density (mW cm ⁻²)	current density (mA cm ⁻²)	references
SPES	80	20.31	75.55	255.71	13
PSPES	80	24.15 ± 1	78.4	260.6	this work
PSPES-HBN1	80	52.3 ± 2.61	176.3	617.2	this work
PSPES-HBN2	80	77.4 ± 3.87	220.3	795.5	this work
PSPES-HBN3	80	65.9 ± 3.29	188.8	704.7	this work
PES-PVP	180	0.06	218		26
mp-S0	150	0.09	361		26
m-PBI350-2	160	0.194	595	~270	40
Acid doped PBI	150	0.034		0.5	81
PTSA@TpAzo	60	7.8 × 10 ⁻² at 80 °C	24	90	95
dABPBI-MSA	150	1.05	242	404	96
dABPBI-TFA	150	1.6	139	222	96
Nafion-117	80	26	350	750	91

interconnect the porous polymer channels and strengthen the compatibility between the electrode and electrolyte interfacial region.^{46,86,91–94}

Furthermore, the large concentration of OH groups in HBN might transport the protons with the neighboring sites of SO₃H in the PSPES-HBN2 polymer matrix, which increases the conductivity of the PSPES-HBN2 membrane and finally enhances the fuel cell performance. PEMFC assembled with pristine PSPES delivered a peak power density of 78.4 mW cm⁻² at a load current density of 260.6 mA cm⁻², whereas PSPES-HBN1, PSPES-HBN2, and PSPES-HBN3 delivered peak power densities of 176.3, 220.3, and 188.8 mW cm⁻² at load current densities of 617.2, 795.5, and 704.7 mA cm⁻², respectively. The prepared PSPES-HBN2 membrane showed the PEMFC performance near the Nafion-117 with a peak power density of 350 mW cm⁻² at a load current density of 750 mA cm⁻².⁹¹ The summary of the porous structured membrane is listed in Table 2 to prove the efficient architecture of the porous network in uplifting membrane performance in fuel cell application.

Inspired by the high proton conductivity and polarization performance of PSPES-HBN2, the durability measurements were taken under the H₂/O₂ fuel cell working conditions in Figure 8b. The chemical stability of PEM from the attack of free radicals is a critical property of the fuel cell performance. The PSPES-HBN2 membrane was chosen to investigate the time-dependent voltage retention at 80 °C for 120 h. As stated earlier, incomplete oxygen reduction on the cathode side is responsible for the production of H₂O₂, and it reacts with traces of metal ions to create HO• and HOO• radicals.^{36,59} Chemical degradation of PEM causes PEM thinning, increasing gas permeability and accelerating OCV decay. After a 120 h run, the total OCV decay of PSPES-HBN2 was found to be 0.047 V, which is highly suitable for PEM operation. After impregnating HBN with PSPES, the pores are insignificant, demonstrating that the HBN is filling the pores and evenly distributed in the PSEPS matrix via the interaction of hydroxyl groups with sulfonic acids.⁶ These are sufficient to act as a barrier for hydrogen diffusion along with the matrix and minimize the free radical attack with sulfonic acids, which boosts the polymer's chemical stability. This superior durability of PSPES-HBN2 also arises from the regenerative radical-scavenging ability of HBN and excellent compatibility with PSPES through hydrogen bond, which can emphasize the working stability result, can be considered very promising.

4. CONCLUSIONS

In summary, we have manifested a new amorphous porous framework of sulfonated poly(ether sulfone) SPES with in-built SO₃H moieties in the aromatic chain. The proton source of HBN was impregnated into the porous structure of PSPES via MNIPI. The porous structure and porosity are effectively tuned by altering the added amount of HBN in the PSPES membrane preparation process. The porous structure and the efficacious interfaces with OH–SO₃H pairs assisted the assembly of well compatible and well-interconnected interfaces between HBN and the PSPES matrix, promoting the accelerated proton conduction and mechanical property via the interpenetrating channels of the PSEPS-HBN membrane. The maximum power density reaches 220.3 mW cm⁻² with good retention until 120 h of durability test in an H₂/O₂ fuel cell at 80 °C with 100% RH. The results disclose that the pore containing PSPES membranes are proficient in operating at full humidity and moderate temperatures and disseminate as a promising candidate in PEMFC.

■ ASSOCIATED CONTENT

Supporting Information

The Supporting Information is available free of charge at <https://pubs.acs.org/doi/10.1021/acs.energyfuels.2c00604>.

¹H NMR spectrum of SPES, Raman spectra of BH and HBN, EDS analysis and elemental mapping of BN and HBN, and cross-sectional EDS analysis with elemental mapping of membranes (PDF)

■ AUTHOR INFORMATION

Corresponding Author

Ramesh Prabhu Manimuthu – Department of Physics, Alagappa University, Karaikudi 630 003, India; orcid.org/0000-0002-6492-868X; Email: rameshprabhum@alagappauniversity.ac.in

Authors

Gayathri Ravi Kumar – Department of Physics, Alagappa University, Karaikudi 630 003, India

Raja Pugalenthi M – Department of Physics, Alagappa University, Karaikudi 630 003, India

Guozhong Cao – Department of Materials Science and Engineering, University of Washington, Seattle, Washington 98195-2120, United States

Complete contact information is available at:

<https://pubs.acs.org/10.1021/acs.energyfuels.2c00604>

Notes

The authors declare no competing financial interest.

ACKNOWLEDGMENTS

The authors would like to acknowledge the financial support from the scheme MHRD-RUSA PHASE-2.0, New Delhi. We also thank the UGC-SAP DRS-III, DST-FIST, and DST-PURSE in Alagappa University for help with the instrumental facility.

REFERENCES

- (1) Bagher, M.; Hooshyari, K.; Salarizadeh, P.; Mohammadi, F. A comprehensive review on the proton conductivity of proton exchange membranes (PEMs) under anhydrous conditions : Proton conductivity upper bound. *Int. J. Hydrogen Energy* **2021**, *46*, 34413–34437.
- (2) Wang, Y.; Ruiz Diaz, D. F.; Chen, K. S.; Wang, Z.; Adroher, X. C. Materials, technological status, and fundamentals of PEM fuel cells – A review. *Mater. Today* **2020**, *32*, 178–203.
- (3) Zhang, H.; Shen, P. K. Recent development of polymer electrolyte membranes for fuel cells. *Chem. Rev.* **2012**, *112*, 2780–2832.
- (4) Cano, Z. P.; Banham, D.; Ye, S.; Hintennach, A.; Lu, J.; Fowler, M.; Chen, Z. Batteries and fuel cells for emerging electric vehicle markets. *Nat. Energy* **2018**, *3*, 279–289.
- (5) Hariprasad, R.; Vinothkannan, M.; Kim, A. R.; Yoo, D. J. SPVdF-HFP/SGO nanohybrid proton exchange membrane for the applications of direct methanol fuel cells. *J. Dispersion Sci. Technol.* **2020**, *42*, 33–45.
- (6) Kim, Y. S. Polymer Electrolytes with High Ionic Concentration for Fuel Cells and Electrolyzers. *ACS Appl. Polym. Mater.* **2021**, *3*, 1250–1270.
- (7) Yin, C.; Li, J.; Zhou, Y.; Zhang, H.; Fang, P.; He, C. Enhancement in proton conductivity and thermal stability in nafion membranes induced by incorporation of sulfonated carbon nanotubes. *ACS Appl. Mater. Interfaces* **2018**, *10*, 14026–14035.
- (8) Pugalenth, R. M.; Manimuthu, R. P. Synergistic effect of polydopamine modified CaZrO₃ perovskite and hydroxylated SPEEK for the acid-base cation exchange membrane fuel cells. *Energy Fuel* **2021**, *35*, 16837–16849.
- (9) kumar, G. G.; Kim, A. R.; Nahm, K. S.; Yoo, D. J.; Elizabeth, R. High ion and lower molecular transportation of the poly vinylidene fluoride-hexa fluoro propylene hybrid membranes for the high temperature and lower humidity direct methanol fuel cell applications. *J. Power Sources* **2010**, *195*, S922–S928.
- (10) Ding, F.; Hu, H.; Ding, H.; Liu, J.; Chen, Y.; Xiao, M.; Meng, Y.; Sun, L. Sulfonated poly(fluorene ether ketone) (SPFEK)/ α -zirconium phosphate (ZrP) nanocomposite membranes for fuel cell applications. *Adv. Compos. Hybrid Mater.* **2020**, *3*, 546–550.
- (11) Hu, H.; Ding, F.; Ding, H.; Liu, J.; Xiao, M.; Meng, Y.; Sun, L. Sulfonated poly(fluorenyl ether ketone)/Sulfonated α -zirconium phosphate Nanocomposite membranes for proton exchange membrane fuel cells. *Adv. Compos. Hybrid Mater.* **2020**, *3*, 498–507.
- (12) Mariappan, R. P.; Cao, G.; Manimuthu, R. P. Cross-linked SPEEK-PEG-APTEOS-modified CaTiO₃ perovskites for efficient acid – base cation-exchange membrane fuel cell. *Energy Fuels* **2020**, *34*, 10087–10099.
- (13) Kumar, G. R.; Guozhong, C.; Manimuthu, R. P. Sandwich assembly of sulfonated poly (ether sulfone) with sulfonated multiwalled carbon nanotubes as an efficient architecture for enhanced electrolyte performance in H₂/O₂ fuel cells. *Int. J. Energy Res.* **2022**, *46*, 2567.
- (14) Martina, P.; Gayathri, R.; Pugalenth, M. R.; Cao, G.; Liu, C.; Prabhu, M. R. Nanosulfonated silica incorporated SPEEK/SPVdF-HFP polymer blend membrane for PEM fuel cell application. *Ionics* **2020**, *26*, 3447–3458.
- (15) Park, C. H.; Lee, C. H.; Guiver, M. D.; Lee, Y. M. Sulfonated hydrocarbon membranes for medium-temperature and low-humidity proton exchange membrane fuel cells (PEMFCs). *Prog. Polym. Sci.* **2011**, *36*, 1443–1498.
- (16) Anahidzade, N.; Abdolmaleki, A.; Dinari, M.; Firouz Tadavani, K.; Zhiani, M. Metal-organic framework anchored sulfonated poly(ether sulfone) as a high temperature proton exchange membrane for fuel cells. *J. Membr. Sci.* **2018**, *565*, 281–292.
- (17) Divya, K.; Rana, D.; Sri Abirami Saraswathi, M. S.; Bhat, S. D.; Shukla, A.; Nagendran, A. Investigation of the versatility of SPES membranes customized with sulfonated molybdenum disulfide nanosheets for DMFC applications. *Int. J. Hydrogen Energy* **2020**, *45*, 15507–15520.
- (18) Gahlot, S.; Sharma, P. P.; Kulshrestha, V.; Jha, P. K. SGO/SPES-based highly conducting polymer electrolyte membranes for fuel cell application. *ACS Appl. Mater. Interfaces* **2014**, *6*, 5595–5601.
- (19) Gayathri, R.; Prabhu, M. R. Protonated state and synergistic role of Nd³⁺ doped barium cerate perovskite for the enhancement of ionic pathways in novel sulfonated polyethersulfone for H₂/O₂ fuel cells. *Soft Matter* **2020**, *16*, 4220–4233.
- (20) Xu, X.; Li, R.; Tang, C.; Wang, H.; Zhuang, X.; Liu, Y.; Kang, W.; Shi, L. Cellulose nanofiber-embedded sulfonated poly (ether sulfone) membranes for proton exchange membrane fuel cells. *Carbohydr. Polym.* **2018**, *184*, 299–306.
- (21) Zhang, C.; Zhuang, X.; Li, X.; Wang, W.; Cheng, B.; Kang, W.; Cai, Z.; Li, M. Chitin nanowhisker-supported sulfonated poly(ether sulfone) proton exchange for fuel cell applications. *Carbohydr. Polym.* **2016**, *140*, 195–201.
- (22) Li, Z.; Liu, Z.; Li, H.; Hasan, M.; Suwansoontorn, A.; Du, G.; Wang, D.; Zhang, Y.; Nagao, Y. sulfonated triazine-based porous organic polymers for excellent proton conductivity. *ACS Appl. Polym. Mater.* **2020**, *2*, 3267–3273.
- (23) Vinothkannan, M.; Kim, A. R.; Gnana, G.; Gnana kumar, J.-M.; Yoo, D. J. Toward improved mechanical strength, oxidative stability and proton conductivity of an aligned quadratic hybrid (SPEEK/FPAPB/Fe₃O₄-FGO) membrane for application in high temperature and low humidity fuel cells. *RSC Adv.* **2017**, *7*, 39034–39048.
- (24) Nam, K.-H.; Seo, K.; Lee, S.; Han, H. Sulfur-doped hierarchically porous open cellular polymer/acid complex electrolyte membranes for efficient water-free proton transport. *ACS Sustain. Chem. Eng.* **2020**, *8*, 16156–16163.
- (25) Liu, X.; Meng, X.; Wu, J.; Huo, J.; Cui, L.; Zhou, Q. Microstructure and properties of novel SPEEK/PVDF-g-PSSA blends for proton exchange membrane with improved compatibility. *RSC Adv.* **2015**, *5*, 69621–69628.
- (26) Guo, Z.; Xiu, R.; Lu, S.; Xu, X.; Yang, S.; Xiang, Y. Submicropore containing poly(ether sulfones)/polyvinylpyrrolidone membranes for high-temperature fuel cell applications. *J. Mater. Chem. A* **2015**, *3*, 8847–8854.
- (27) Zhou, D.; Li, D.; Liu, M.; Zhong, X.; Wei, H.; Wang, Z.; Jiang, Q.; Jin, F.; Cui, D. Experimental Parameters Affecting Cross-Linking Density and Free-Thaw Stability of Cross-Linked Porous Starch. *ES Food Agrofor.* **2021**, *5*, 20–28.
- (28) Peng, Z.; Jiang, Q.; Peng, P.; Li, F. NH₃-activated fullerene derivative hierarchical microstructures to porous Fe₃O₄/N-C for oxygen reduction reaction and Zn-air battery. *Eng. Sci.* **2021**, *14*, 27–38.
- (29) Zhang, D.; Li, S.; Li, Y.; Mei, N.; Pu, H.; Jiao, S. Numerical Investigation on the Mechanism of Multicomponent Boiling in Porous Media Using LBM at Pore Scale. *ES Energy Environ.* **2021**, *12*, 108–116.
- (30) Iwe, I. A.; Gosteva, E. A.; Starkov, V. V.; Sedlovets, D. M.; Mong, O. Anti-Glare Coatings Based on Porous Silicon Structures. *ES Mater. Manuf.* **2019**, *3*, 47–51.
- (31) Hao, Q.; Xiao, Y.; Medina, F. J. Annealing Studies of Nanoporous Si Thin Films Fabricated by Dry Etch. *ES Mater. Manuf.* **2019**, *6*, 24–27.

- (32) Xiao, Y.; Chen, Q.; Ma, D.; Yang, N.; Hao, Q. Phonon Transport within Periodic Porous Structures — From Classical Phonon Size Effects to Wave Effects. *ES Mater. Manuf.* **2019**, *5*, 2–18.
- (33) Bag, P. P.; Singh, G. P.; Singha, S.; Roymahapatra, G. Synthesis of metal-organic frameworks (MOFs) and their biological, catalytic and energetic applications: A mini review. *Eng. Sci.* **2021**, *13*, 1–10.
- (34) Yu, H.; Xu, C.; Li, Y.; Jin, F.; Ye, F.; Li, X. Performance Enhancement of CuO/ZnO by Deposition on the Metal-Organic Framework of Cu-BTC for Methanol Steam Reforming Reaction. *ES Energy Environ.* **2020**, *8*, 65–77.
- (35) Nong, W.; Liu, X.; Wang, Q.; Wu, J.; Guan, Y. Metal-organic Framework-based Materials: Synthesis, Stability and Applications in Food Safety and Preservation. *ES Food Agrofor.* **2020**, *1*, 11–40.
- (36) Kallem, P.; Drobek, M.; Julbe, A.; Vriezolk, E. J.; Mallada, R.; Pina, M. P. Hierarchical Porous Polybenzimidazole Microsieves: An Efficient Architecture for Anhydrous Proton Transport via Polyionic Liquids. *ACS Appl. Mater. Interfaces* **2017**, *9*, 14844–14857.
- (37) Hazarika, M.; Jana, T. Proton exchange membrane developed from novel blends of polybenzimidazole and poly(vinyl-1,2,4-triazole). *ACS Appl. Mater. Interfaces* **2012**, *4*, S256–S265.
- (38) Langevin, D.; Nguyen, Q. T.; Marais, S.; Karademir, S.; Sanchez, J.-Y.; Iojoiu, C.; Martinez, M.; Mercier, R.; Judeinstein, P.; Chappey, C. High-temperature ionic-conducting material: Advanced structure and improved performance. *J. Phys. Chem. C* **2013**, *117*, 15552–15561.
- (39) Kang, D. W.; Song, J. H.; Lee, K. J.; Lee, H. G.; Kim, J. E.; Lee, H. Y.; Kim, J. Y.; Hong, C. S. Conductive porous organic polymer with superprotonic conductivity of a Nafion-type electrolyte. *J. Mater. Chem. A* **2017**, *5*, 17492–17498.
- (40) Lee, S.; Nam, K. H.; Seo, K.; Kim, G.; Han, H. Phase inversion-induced porous polybenzimidazole fuel cell membranes: An efficient architecture for high-temperature water-free proton transport. *Polymers* **2020**, *12*, 1604.
- (41) Wang, S.; Zhao, C.; Ma, W.; Zhang, G.; Liu, Z.; Ni, J.; Li, M.; Zhang, N.; Na, H. Preparation and properties of epoxy-cross-linked porous polybenzimidazole for high temperature proton exchange membrane fuel cells. *J. Membr. Sci.* **2012**, *411–412*, 54–63.
- (42) Kang, D. W.; Kang, M.; Hong, C. S. Post-synthetic modification of porous materials: Superprotonic conductivities and membrane applications in fuel cells. *J. Mater. Chem. A* **2020**, *8*, 7474–7494.
- (43) Yu, C.; Zhang, J.; Tian, W.; Fan, X.; Yao, Y. Polymer composites based on hexagonal boron nitride and their application in thermally conductive composites. *RSC Adv.* **2018**, *8*, 21948–21967.
- (44) Yadav, V.; Kulshrestha, V. Boron nitride: A promising material for proton exchange membranes for energy applications. *Nanoscale* **2019**, *11*, 12755–12773.
- (45) Wang, J.; Ma, F.; Sun, M. Graphene, hexagonal boron nitride, and their heterostructures: properties and applications. *RSC Adv.* **2017**, *7*, 16801–16822.
- (46) Yoon, S. I.; Ma, K. Y.; Kim, T.-Y.; Shin, H. S. Proton conductivity of a hexagonal boron nitride membrane and its energy applications. *J. Mater. Chem. A* **2020**, *8*, 2898–2912.
- (47) Liu, H.; Yan, Z.; Sun, Z.; Li, A.; Guo, Z.; Qian, L. Highly Efficient Synthesis of Hexagonal Boron Nitride Nanofibers with High Specific Surface Area. *ES Mater. Manuf.* **2021**, *16*, 56–65.
- (48) Liu, C.; Fang, Q.; Wang, D.; Yan, C.; Liu, F.; Wang, N.; Guo, Z.; Jiang, Q. Carbon and Boron Nitride Nanotubes: Structure, Property and Fabrication. *ES Mater. Manuf.* **2019**, *3*, 2–15.
- (49) Ivanova, M. N.; Grayfer, E. D.; Plotnikova, E. E.; Kibis, L. S.; Darabdhara, G.; Boruah, P. K.; Das, M. R.; Fedorov, V. E. Pt-Decorated Boron Nitride Nanosheets as Artificial Nanozyme for Detection of Dopamine. *ACS Appl. Mater. Interfaces* **2019**, *11*, 22102–22112.
- (50) Gahlot, S.; Kulshrestha, V. White graphene based composite proton exchange membrane: Improved durability and proton conductivity. *Int. J. Hydrogen Energy* **2018**, *43*, 21683–21689.
- (51) Bai, L.; Zheng, S.; Bao, R.; Liu, Z.; Yang, M.; Yang, W. Effect of PLA Crystallization on the Thermal Conductivity and Breakdown Strength of PLA/BN Composites. *ES Mater. Manuf.* **2018**, *3*, 66–72.
- (52) Pan, D.; Zhang, X.; Yang, G.; Shang, Y.; Su, F.; Hu, Q.; Patil, R. R.; Liu, H.; Liu, C.; Guo, Z. Thermally Conductive Anticorrosive Epoxy Nanocomposites with Tannic Acid-Modified Boron Nitride Nanosheets. *Ind. Eng. Chem. Res.* **2020**, *59*, 20371–20381.
- (53) Pan, D.; Su, F.; Liu, H.; Ma, Y.; Das, R.; Hu, Q.; Liu, C.; Guo, Z. The Properties and Preparation Methods of Different Boron Nitride Nanostructures and Applications of Related Nanocomposites. *Chem. Rec.* **2020**, *20*, 1314.
- (54) Pan, D.; Dong, J.; Yang, G.; Su, F.; Chang, B.; Liu, C.; Zhu, Y.-C.; Guo, Z. Ice template method assists in obtaining carbonized cellulose/boron nitride aerogel with 3D spatial network structure to enhance the thermal conductivity and flame retardancy of epoxy-based composites. *Adv. Compos. Hybrid Mater.* **2021**, *5*, 58–70.
- (55) Wu, X.; Su, C.; Shi, K.; Wu, F.; Fu, C. Coupling Between Hyperbolic Phonon Polaritons Excited in Two Ultrathin Hexagonal Boron Nitride Sheets. *Eng. Sci.* **2022**, *5*, 21–29.
- (56) Jia, W.; Tang, B.; Wu, P. Novel Composite Proton Exchange Membrane with Connected Long-Range Ionic Nanochannels Constructed via Exfoliated Na fi on – Boron Nitride Nanocomposite. *ACS Appl. Mater. Interfaces* **2017**, *9*, 14791–14800.
- (57) Akel, M.; Ünügür Çelik, S.; Bozkurt, A.; Ata, A. Nano Hexagonal Boron Nitride–Nafion Composite Membranes for Proton Exchange Membrane Fuel Cells. *Polym. Compos.* **2014**, *37*, 422–428.
- (58) Ulus, H.; Üstün, T.; Eskizeybek, V.; Şahin, Ö. S.; Avcı, A.; Ekrem, M. Boron nitride-MWCNT/epoxy hybrid nanocomposites: Preparation and mechanical properties. *Appl. Surf. Sci.* **2014**, *318*, 37–42.
- (59) Oh, K.-H.; Lee, D.; Choo, M.-J.; Park, K. H.; Jeon, S.; Hong, S. H.; Park, J.-K.; Choi, J. W. Enhanced Durability of Polymer Electrolyte Membrane Fuel Cells by Functionalized 2D Boron Nitride Nano flakes. *ACS Appl. Mater. Interfaces* **2014**, *6*, 7751–7758.
- (60) Yadav, V.; Rajput, A.; Rathod, N. H.; Kulshrestha, V. Enhancement in proton conductivity and methanol cross-over resistance by sulfonated boron nitride composite sulfonated poly(ether ether ketone) proton exchange membrane. *Int. J. Hydrogen Energy* **2020**, *45*, 17017–17028.
- (61) Guan, R.; Dai, H.; Li, C.; Liu, J.; Xu, J. Effect of casting solvent on the morphology and performance of sulfonated polyethersulfone membranes. *J. Membr. Sci.* **2006**, *277*, 148–156.
- (62) Dai, H.; Guan, R.; Li, C.; Liu, J. Development and characterization of sulfonated poly(ether sulfone) for proton exchange membrane materials. *Solid State Ionics* **2007**, *178*, 339–345.
- (63) Athira, V. B.; Mohanty, S.; Nayak, S. K. Preparation and characterization of porous polyethersulfone (PES) membranes with improved biocompatibility by blending sulfonated polyethersulfone (SPES) and cellulose acetate (CA) – A comparative study. *Mater. Today Commun.* **2020**, *25*, 101544.
- (64) Bhran, A.; Shoaib, A.; Elsaied, D.; El-gendi, A.; Abdallah, H. Preparation of PVC/PVP composite polymer membranes via phase inversion process for water treatment purposes. *Chin. J. Chem. Eng.* **2018**, *26*, 715–722.
- (65) Mittal, G.; Rhee, K. Y.; Park, S. J. Processing and Characterization of PMMA/PI Composites Reinforced With Surface Functionalized Hexagonal Boron Nitride. *Appl. Surf. Sci.* **2017**, *415*, 49–54.
- (66) Elakkiya, S.; Arthanareeswaran, G.; Venkatesh, K.; Kweon, J. Enhancement of fuel cell properties in polyethersulfone and sulfonated poly(ether ether ketone) membranes using metal oxide nanoparticles for proton exchange membrane fuel cell. *Int. J. Hydrogen Energy* **2018**, *43*, 21750–21759.
- (67) Kim, A. R.; Park, C. J.; Vinothkannan, M.; Yoo, D. J. Sulfonated poly ether sulfone/heteropoly acid composite membranes as electrolytes for the improved power generation of proton exchange membrane fuel cells. *Composites, Part B* **2018**, *155*, 272–281.
- (68) Shi, Y.; Hamsen, C.; Jia, X.; Kim, K. K.; Reina, A.; Hofmann, M.; Hsu, A. L.; Zhang, K.; Li, H.; Juang, Z.-Y.; Dresselhaus, M. S.; Li, L.-J.; Kong, J. Synthesis of few-layer hexagonal boron nitride thin film by chemical vapor deposition. *Nano Lett.* **2010**, *10*, 4134–4139.

- (69) Pan, D.; Luo, S.; Feng, Y.; Zhang, X.; Su, F.; Liu, H.; Liu, C.; Mai, X.; Naik, N.; Guo, Z. Highly thermally conductive 3D BN/MWCNTs/C spatial network composites with improved electrically insulating and flame retardancy prepared by biological template assisted method. *Composites, Part B* **2021**, *222*, 109039.
- (70) Gahlot, S.; Gupta, H.; Jha, P. K.; Kulshrestha, V. Enhanced Electrochemical Performance of Stable SPES/SPANI Composite Polymer Electrolyte Membranes by Enriched Ionic Nanochannels. *ACS Omega* **2017**, *2*, 5831–5839.
- (71) Lee, D.; Song, S. H. Ultra-thin ultraviolet cathodoluminescent device based on exfoliated hexagonal boron nitride. *RSC Adv.* **2017**, *7*, 7831–7835.
- (72) Galbiati, S.; Baricci, A.; Casalegno, A.; Marchesi, R. Degradation in phosphoric acid doped polymer fuel cells: A 6000 h parametric investigation. *Int. J. Hydrogen Energy* **2013**, *38*, 6469–6480.
- (73) Rambabu, G.; Nagaraju, N.; Bhat, S. D. Functionalized fullerene embedded in Nafion matrix: A modified composite membrane electrolyte for direct methanol fuel cells. *Chem. Eng. J.* **2016**, *306*, 43–52.
- (74) Jang, H.-R.; Yoo, E.-S.; Kannan, R.; Kim, J.-S.; Lee, K.; Yoo, D. J. Facile tailor-made enhancement in proton conductivity of sulfonated poly(ether ether ketone) by graphene oxide nanosheet for polymer electrolyte membrane fuel cell applications. *Colloid Polym. Sci.* **2017**, *295*, 1059–1069.
- (75) Liu, H.; Guo, L.; Liu, M.; Chen, H.; Han, W.; Bian, H.; Tian, X.; Wang, C.; Guo, Z.; Sun, J. Water Management Simulation of Proton Exchange Membrane Fuel Cells with Micro-ribs Based on Volume of Fluid Model. *ES Energy Environ.* **2022**, *15*, 45–55.
- (76) Wang, B.; Sun, X.; Xie, X.; Wang, J.; Li, L.; Jiao, K. Experimental Investigation of a Novel Cathode Matrix Flow Field in Proton Exchange Membrane Fuel Cell. *ES Energy Environ.* **2021**, *12*, 95–107.
- (77) Li, W.; Tang, Z.; Tam, V. W. Y.; Zhao, X.; Wang, K. A Review on Durability of Alkali-activated System from Sustainable Construction Materials to Infrastructures. *ES Mater. Manuf.* **2019**, *4*, 2–19.
- (78) Elayappan, V.; Murugadoss, V.; Fei, Z.; Dyson, P. J.; Angaiah, S. Influence of polypyrrole incorporated electrospun poly(vinylidene fluoride-co-hexafluoropropylene) nanofibrous composite membrane electrolyte on the photovoltaic performance of dye sensitized solar cell. *Eng. Sci.* **2020**, *10*, 78–84.
- (79) Yamaguchi, T.; Ibe, M.; Nair, B. N.; Nakao, S.-i. A Pore-Filling Electrolyte Membrane-Electrode Integrated System for a Direct Methanol Fuel Cell Application. *J. Electrochem. Soc.* **2002**, *149*, A1448.
- (80) Bi, C.; Zhang, H.; Xiao, S.; Zhang, Y.; Mai, Z.; Li, X. Grafted porous PTFE/partially fluorinated sulfonated poly(arylene ether ketone) composite membrane for PEMFC applications. *J. Membr. Sci.* **2011**, *376*, 170–178.
- (81) Li, J.; Li, X.; Yu, S.; Hao, J.; Lu, W.; Shao, Z.; Yi, B. Porous polybenzimidazole membranes doped with phosphoric acid: Preparation and application in high-temperature proton-exchange-membrane fuel cells. *Energy Convers. Manag.* **2014**, *85*, 323–327.
- (82) Shen, C.-H.; Jheng, L.-c.; Hsu, S. L.-c.; Tse-Wei Wang, J. Phosphoric acid-doped cross-linked porous polybenzimidazole membranes for proton exchange membrane fuel cells. *J. Mater. Chem.* **2011**, *21*, 15660–15665.
- (83) Kim, A. R.; Vinothkannan, M.; Lee, K. H.; Chu, J. Y.; Park, B. H.; Han, M. K.; Yoo, D. J. Enhanced performance and durability of composite membranes containing anatase titanium oxide for fuel cells operating under low relative humidity. *Int. J. Energy Res.* **2022**, *46*, 4835–4851.
- (84) Alenazi, N. A.; Hussein, M. A.; Alamry, K. A.; Asiri, A. M. Modified polyether-sulfone membrane: a mini review. *Des. Monomers Polym.* **2017**, *20*, 532–546.
- (85) Rahimpour, A.; Madaeni, S. S.; Ghorbani, S.; Shockravi, A.; Mansourpanah, Y. The influence of sulfonated polyethersulfone (SPES) on surface nano-morphology and performance of polyethersulfone (PES) membrane. *Appl. Surf. Sci.* **2010**, *256*, 1825–1831.
- (86) Pugalenth, M. R.; Gayathri, R.; Cao, G.; Prabhu, M. R. Study of amine customized exfoliated BN sheets in SPEEK-PES based blend membrane for acid-base cation exchange membrane fuel cells. *J. Chem. Environ. Eng.* **2022**, *10*, 107025.
- (87) Wang, H.; Wang, X.; Fan, T.; Zhou, R.; Li, J.; Long, Y.; Zhuang, X.; Cheng, B. Fabrication of electrospun sulfonated poly(ether sulfone) nanofibers with amino modified SiO₂ nanosphere for optimization of nanochannels in proton exchange membrane. *Solid State Ionics* **2020**, *349*, 115300.
- (88) Jia, W.; Wu, P. Stable boron nitride nanocomposites based membranes for high-efficiency proton conduction. *Electrochim. Acta* **2018**, *273*, 162–169.
- (89) Kim, A. R.; Vinothkannan, M.; Kim, J. S.; Yoo, D. J. Proton-conducting phosphotungstic acid/sulfonated fluorinated block copolymer composite membrane for polymer electrolyte fuel cells with reduced hydrogen permeability. *Polym. Bull.* **2018**, *75*, 2779–2804.
- (90) Vinothkannan, M.; Ramakrishnan, S.; Kim, A. R.; Lee, H.-K.; Yoo, D. J. Ceria Stabilized by Titanium Carbide as a Sustainable Filler in the Nafion Matrix Improves the Mechanical Integrity, Electrochemical Durability, and Hydrogen Impermeability of Proton-Exchange Membrane Fuel Cells: Effects of the Filler Content. *ACS Appl. Mater. Interfaces* **2020**, *12*, 5704–5716.
- (91) Martínez-Casillas, D.; Solorza, O.; Mollá, S.; Montero, Á.; García-Bernabé, A.; Compañ, V. Polymer modified sulfonated PEEK ionomers membranes and the use of Ru₃Pd₆Pt as cathode catalyst for H₂/O₂ fuel cells. *Int. J. Hydrogen Energy* **2019**, *44*, 295–303.
- (92) Guo, Y.; Xu, J.; Lan, C.; Bi, K. Broadband and high-efficiency linear polarization converter based on reflective metasurface. *Eng. Sci.* **2021**, *14*, 39–45.
- (93) Wu, X.; Fu, C.; Zhang, Z. M. Chiral Absorbers Based on Polarization Conversion and Excitation of Magnetic Polaritons. *ES Energy Environ.* **2020**, *8*, 5–14.
- (94) Dizaji, M. T.; Li, W. Higher voltage redox flow batteries with hybrid acid and base electrolytes. *Eng. Sci.* **2020**, *11*, 54–65.
- (95) Sasmal, H. S.; Aiyappa, H. B.; Bhange, S. N.; Karak, S.; Halder, A.; Kurungot, S.; Banerjee, R. Superprotonic Conductivity in Flexible Porous Covalent Organic Framework Membranes. *Angew. Chem., Int. Ed.* **2018**, *57*, 10894–10898.
- (96) Nayak, R.; Sundarraman, M.; Ghosh, P. C.; Bhattacharyya, A. R. Doped poly(2,5-benzimidazole) membranes for high temperature polymer electrolyte fuel cell: Influence of various solvents during membrane casting on the fuel cell performance. *Eur. Polym. J.* **2018**, *100*, 111–120.